AGU PUBLICATIONS

Geophysical Research Letters

RESEARCH LETTER
10.1002/2018GL077021

Key Points:
- The constant flux layer assumption does not necessarily require turbulent transport to be symmetric
- The constant flux layer assumption imposes intrinsic constraints on the eddy structure in the lower atmosphere
- The structural model provides a new perspective on closing triple moments and diagnosing constant flux layer from single-level measurements

Supporting Information:
- Supporting Information S1

Correspondence to:
D. Li,
lidan@bu.edu

Citation:
Li, D., Katul, G. G., & Liu, H. (2018). Intrinsic constraints on asymmetric turbulent transport of scalars within the constant flux layer of the lower atmosphere. *Geophysical Research Letters*, *45*. https://doi.org/10.1002/2018GL077021

Received 5 JAN 2018
Accepted 1 FEB 2018
Accepted article online 7 FEB 2018

Intrinsic Constraints on Asymmetric Turbulent Transport of Scalars Within the Constant Flux Layer of the Lower Atmosphere

Dan Li[1], **Gabriel G. Katul**[2], **and Heping Liu**[3]

[1]Department of Earth and Environment, Boston University, Boston, MA, USA, [2]Nicholas School of the Environment and Department of Civil and Environmental Engineering, Duke University, Durham, NC, USA, [3]Department of Civil and Environmental Engineering, Washington State University, Pullman, WA, USA

Abstract A widely used assumption in boundary layer meteorology is the z independence of turbulent scalar fluxes F_s throughout the atmospheric surface layer, where z is the distance from the boundary. This assumption is necessary for the usage of Monin-Obukhov Similarity Theory and for the interpretation of eddy covariance measurements of F_s when using them to represent emissions or uptake from the surface. It is demonstrated here that the constant flux assumption offers intrinsic constraints on the third-order turbulent transport of F_s in the unstable atmospheric surface layer. When enforcing z independence of F_s on multilevel F_s measurements collected above different surface cover types, it is shown that increasing instability leads to a novel and universal description of (i) the imbalance between ejecting and sweeping eddy contributions to F_s and (ii) the ratio formed by a dimensionless turbulent transport of F_s and a dimensionless turbulent transport of scalar variance. When combined with structural models for the turbulent transport of F_s, these two findings offer a new perspective on "closing" triple moments beyond conventional gradient diffusion schemes. A practical outcome is a diagnostic of the constant flux assumption from single-level F_s measurements.

1. Introduction

In an idealized atmospheric surface layer (ASL), the turbulent flux F_s of a scalar entity s is z independent and is given by the emission or uptake rate from the surface, where z is the height above the ground (or a zero-plane displacement for canopies). This assumption is essential for interpreting eddy covariance measurements when they are used to represent surface fluxes (Baldocchi et al., 2001). It is also a necessary condition for the applicability of Monin-Obukhov Similarity Theory (MOST) (Monin & Obukhov, 1954), which is common to all parametrizations of surface atmosphere gas exchanges in weather and climate models (Stensrud, 2007). For any scalar s (e.g., potential temperature θ, water vapor q, and CO_2), the attainment of a "constant flux" layer (i.e., $\partial F_s/\partial z = 0$, where $F_s = \overline{w's'}$) can be derived from the budget equation for $\bar{s}$ subject to what can be labeled as "idealized" conditions. These conditions necessitate that the ASL flow is stationary and planar homogeneous at sufficiently large Reynolds and Peclet numbers with no large-scale subsidence (Garratt, 1992; Stull, 1988). Here and throughout, u, v, and w are instantaneous longitudinal, lateral, and vertical velocity components along Cartesian coordinates x, y, and z, respectively, t is time, overbar indicates time-averaging, and primed quantities denote turbulent fluctuations around the time-averaged state. The representative scalar s is assumed to be θ throughout, and extensions to other scalars such as q are discussed in the supporting information.

During daytime conditions, the ASL interacts with an overlying convective boundary layer (CBL), a layer characterized by a vertically well-mixed $\bar{\theta}$ (i.e., $\partial\bar{\theta}/\partial z = 0$) due to the role of large-scale eddies (Garratt, 1992; Stull, 1988). The CBL, however, cannot maintain a stationary $\bar{\theta}$ necessitating a revision to the mean scalar continuity equation, now given by

$$\frac{\partial\bar{\theta}}{\partial t} = -\frac{\partial\overline{w'\theta'}}{\partial z}. \tag{1}$$

Upon differentiating equation (1) with respect to z and enforcing $\partial\bar{\theta}/\partial z = 0$, the mean scalar continuity equation in the CBL reduces to

$$-\frac{\partial^2\overline{w'\theta'}}{\partial z^2} = 0. \tag{2}$$

Twice-integrating equation (2) with respect to z leads to the common linear flux profile connecting $F_s = \overline{w'\theta'}$ in the ASL to $\overline{w'\theta'}$ at the top of the CBL (i.e., the entrainment flux). As the instability increases, the ASL and the CBL become increasingly coupled, casting doubts on the validity of the constant flux layer assumption. The coupling between the ASL and the CBL originates from large-scale eddies in the well-mixed CBL impinging on the ASL. A number of features about these eddies have now been reasonably established. They contribute to $\overline{w'\theta'}$ throughout the atmospheric boundary layer (including the ASL), and they do not abide by gradient diffusion arguments of the form $\overline{w'\theta'} \propto \partial\bar{\theta}/\partial z$ as reviewed elsewhere (Ghannam et al., 2017; Holtslag & Moeng, 1991; Holtslag & Boville, 1993; van Dop & Verver, 2001; Zilitinkevich et al., 1999). Moreover, contributions to F_s from ejections and sweeps become increasingly imbalanced (Katul, Kuhn, et al., 1997; Li & Bou-Zeid, 2011) with increasing instability. Ejections and sweeps are two types of coherent eddy motions that are commonly delineated by conditional sampling and quadrant analysis (Wallace, 2016) applied to w' and θ'. One implication of such imbalance between sweeps and ejections is that the third-order turbulent transport of F_s (i.e., $\overline{w'w'\theta'}$) becomes locally asymmetric (Ghannam et al., 2017). Asymmetric transport here refers to flux contributions by ejections and sweeps being not identical. This definition is related to but not identical to the definition in earlier studies (Wyngaard, 1985; Wyngaard & Weil, 1991) referring to the asymmetry between "bottom-up" and "top-down" diffusion processes. Can the ASL still satisfy the constant flux assumption under the influence of such asymmetric transport induced by large eddies? More importantly, does maintaining $\partial\overline{w'\theta'}/\partial z = 0$ in the ASL impose any constraints on the behavior of $\overline{w'w'\theta'}$ and its gradient with increasing instability? Answering these questions frames the scope of this study.

To address these questions, a link between $\overline{w'w'\theta'}$, its gradient, coherent structures and their asymmetric signature in sweep-ejection events, and F_s must be developed. The theoretical underpinning to building such a link is the so-called structural parameterization of $\overline{w'w'\theta'}$ as discussed elsewhere (Fer et al., 2004; Nagano & Tagawa, 1988, 1990). Conventional turbulence closure schemes (Katul et al., 2001; Meyers & Paw U, 1987; Siqueira & Katul, 2002) that relate $\overline{w'w'\theta'}$ to $\partial\overline{w'\theta'}/\partial z$ predict $\overline{w'w'\theta'} = 0$ when $\partial\overline{w'\theta'}/\partial z = 0$ is maintained in the ASL. That is, conventional turbulence closure schemes fail to offer any "realistic" constraint on $\overline{w'w'\theta'}$ in a constant flux ASL (other than their complete absence). However, structural models relate $\overline{w'w'\theta'}$ to $\overline{w'\theta'}$ while accounting for some characteristics of coherent motions such as ejections and sweeps based on dimensional analysis and other considerations. These structural models are given as $\overline{w'w'\theta'} \propto \overline{w'\theta'}$ and have been proposed for the CBL as discussed elsewhere (Abdella & McFarlane, 1997; Canuto et al., 1994; Gryanik & Hartmann, 2002). Structural models derived from third-order cumulant expansions of the joint probability density function of w' and u' or θ' have been successful in describing triple moments for momentum/scalars in canopy flows (Cava et al., 2006; Poggi et al., 2004), ASL and CBL flows (Ghannam et al., 2017; Katul, Kuhn, et al., 1997; Katul, Hsieh, et al., 1997), boundary layers below ice sheets (Fer et al., 2004), and flows over complex topography (Francone et al., 2012; Poggi & Katul, 2007). The work here further develops and employs structural models for scalars to identify the constraints on the ejection-sweep asymmetry and other properties of triple moments when $\partial\overline{w'\theta'}/\partial z = 0$ is a priori imposed on the ASL. Using a combination of data analysis and model derivation, it is shown that $\partial\overline{w'\theta'}/\partial z = 0$ results in a universal scaling for the imbalance between sweep and ejection contributions to F_s with increasing instability.

2. Theory

Unless otherwise stated, an idealized ASL flow with $\partial\overline{w'u'}/\partial z = 0$ is assumed. Also, the momentum flux at the boundary is assumed to be finite and represented by the squared friction velocity $u_*^2 = \tau/\rho$, where $\tau > 0$ is the surface drag and ρ is the mean air density. As such, the free convection regime where $u_* = 0$ is not considered.

2.1. Constant Flux Layer and Nonlocal Transport

The budget equation for the turbulent heat flux $\overline{w'\theta'}$ is given by (Stull, 1988)

$$\frac{\partial\overline{w'\theta'}}{\partial t} = 0 = -\overline{w'w'}\Gamma - \frac{\partial\overline{w'w'\theta'}}{\partial z} - \frac{1}{\rho}\overline{\theta'\frac{\partial p'}{\partial z}} + \beta\overline{\theta'\theta'}. \tag{3}$$

The terms on the right-hand side of equation (3) represent (in order) a production term due to the presence of a mean potential temperature gradient ($\Gamma = \partial\bar{\theta}/\partial z$), a term that represents the third-order turbulent transport of heat flux (also called a turbulent flux transport term), a pressure decorrelation term due to interactions between pressure (p) and temperature, and a buoyancy term arising from thermal stratification ($\beta = g/\bar{\theta}$ and

g is the gravitational acceleration). For s other than θ, the buoyancy term involves the covariance $\overline{\theta' s'}$ instead of $\overline{\theta'\theta'}$. The molecular destruction term is not listed in equation (3) as this term is much smaller than the pressure decorrelation term (Katul et al., 2013, 2014; Stull, 1988). In contrast to equation (1), equation (3) applies to the ASL and CBL without modifications (i.e., $\partial\overline{w'\theta'}/\partial t = 0$ is acceptable in both layers).

The Rotta model (Rotta, 1951) is now invoked for parametrization of the pressure decorrelation term (Moeng & Wyngaard, 1986; Mellor & Yamada, 1974, 1982; Pope, 2000; Yamada, 1975). A Rotta model that retains the linear (or slow) component and the buoyancy component (Moeng & Wyngaard, 1986; Yamada, 1975) is used

$$-\frac{1}{\rho}\overline{\theta'\frac{\partial p'}{\partial z}} = -\frac{\overline{w'\theta'}}{\tau_\theta} - \alpha_1\beta\overline{\theta'\theta'}, \tag{4}$$

where τ_θ is a relaxation time scale that indicates how fast a turbulent eddy loses its coherency and α_1 is a constant (Ghannam et al., 2017). Substituting equation (4) into equation (3) leads to

$$\overline{w'\theta'} = \tau_\theta\left(-\overline{w'w'}\Gamma + \alpha\beta\overline{\theta'\theta'} - \frac{\partial\overline{w'w'\theta'}}{\partial z}\right), \tag{5}$$

where $\alpha = 1-\alpha_1$. This equation shows that $\overline{w'\theta'}$ includes a gradient diffusion term, a buoyancy distortion term, and a turbulent flux transport term that requires closure. It also shows that when $\Gamma = 0$ in the CBL, $\overline{w'\theta'}$ must be due to the buoyancy and the turbulent flux transport terms.

A parameterization for $\overline{w'w'\theta'}$ is now discussed. Traditional turbulent closure schemes parametrize $\overline{w'w'\theta'}$ as a function of $\partial\overline{w'\theta'}/\partial z$. These closure schemes predict $\overline{w'w'\theta'} = 0$ when $\partial\overline{w'\theta'}/\partial z = 0$. However, many studies report finite $\overline{w'w'\theta'}$ (Ghannam et al., 2017). An alternative to gradient diffusion closure is structural parameterizations (Nagano & Tagawa, 1988, 1990) based on cumulant expansion methods. For a third-order cumulant expansion of the joint probability density function of w' and θ' (i.e., only asymmetry is retained as the main deviation from Gaussian joint probability density function), it can be shown that $\overline{w'w'\theta'} = fu_*\overline{w'\theta'}$. The connection between f and characteristics of coherent structures will be elaborated upon in section 2.2. It suffices to state here that $\overline{w'w'\theta'} \propto \overline{w'\theta'}$ has been used in CBL studies before though the relation between the proportionality constant and the flow statistics varies among studies (Ghannam et al., 2017). Substituting $\overline{w'w'\theta'} = fu_*\overline{w'\theta'}$ into equation (5) yields

$$f\frac{\partial\overline{w'\theta'}}{\partial z} + \left(\frac{\partial f}{\partial z} + \frac{1}{\tau_\theta u_*}\right)\overline{w'\theta'} = \frac{-\overline{w'w'}\Gamma + \alpha\beta\overline{\theta'\theta'}}{u_*}. \tag{6}$$

Connections between the constant flux condition and the turbulent flux transport term are now explored for cases that satisfy the following three conditions: (1) the third-order term $\overline{w'w'\theta'}$ is identically zero (i.e., $f = 0$), (2) the normalized vertical velocity variance, the normalized potential temperature variance, and the normalized mean potential temperature gradient are only functions of the stability parameter $\zeta = -z/L$ (L is the Obukhov length) described by MOST, and (3) the τ_θ is chosen so that a constant flux layer is attained when the aforementioned two conditions are satisfied. Multiplying equation (6) by $\kappa_v z/(u_*^2\theta_*)$, where u_* is again the friction velocity assumed finite and constant with z and $\theta_* = -(\overline{w'\theta'})_s/u_*$, is the surface temperature scale, and introducing $h = \overline{w'\theta'}/(\overline{w'\theta'})_s$ result in

$$f\frac{\partial h}{\partial z} + \left(\frac{\partial f}{\partial z} + \frac{1}{\tau_\theta u_*}\right)h = \frac{\phi_{ww}^2\phi_h + \alpha\zeta\phi_{\theta\theta}^2}{\kappa_v z}, \tag{7}$$

where $\phi_{ww} = \sigma_w/u_*$, $\phi_{\theta\theta} = \sigma_\theta/\theta_*$, and $\phi_h = (\kappa_v z/\theta_*)\Gamma$. The functions ϕ_{ww}, ϕ_h, and $\phi_{\theta\theta}$ have been shown to reasonably follow MOST (Garratt, 1992). More importantly, these functions do not affect the key results as shall be seen later. The u_* and θ_* are defined at the surface (or canopy top) and are not functions of z. When $\overline{w'w'\theta'} = 0$, or equivalently, $f = 0$,

$$h = \frac{\tau_\theta u_*}{\kappa_v z}\left[\phi_{ww}^2\phi_h - (\alpha)\zeta\phi_{\theta\theta}^2\right]. \tag{8}$$

In the ASL, $\tau_\theta u_*/\kappa_v z = g_1(\zeta)$ may be interpreted as a dimensionless time scale that varies with atmospheric stability via a similarity function $g_1(\zeta)$ resulting in

$$h = g_1(\zeta)\left[\phi_{ww}^2\phi_h - \alpha\zeta\phi_{\theta\theta}^2\right]. \tag{9}$$

To ensure a constant flux layer (or $h = 1$) for any ζ,

$$g_1(\zeta) = \left[\phi_{ww}^2\phi_h - \alpha\zeta\phi_{\theta\theta}^2\right]^{-1}. \tag{10}$$

The cases where $|f| > 0$ are now considered while maintaining ϕ_{ww}, ϕ_h, and $\phi_{\theta\theta}$ to be only functions of ζ as before. Under such conditions, $\tau_\theta u_*/\kappa_v z = g_2(\zeta)$ is further assumed. The g_2 depends on ζ but can differ from g_1 as the finite turbulent flux transport term may interact with the relaxation time scale of the Rotta model. With these assumptions,

$$\kappa_v z f\frac{\partial h}{\partial z} + \left(\kappa_v z\frac{\partial f}{\partial z} + \frac{1}{g_2}\right)h = \frac{1}{g_1}. \tag{11}$$

From the above equation, a necessary condition for $h = 1$ is

$$\kappa_v\zeta\frac{\partial f}{\partial\zeta} = \frac{1}{g_1} - \frac{1}{g_2}. \tag{12}$$

Here the identity $z(\partial f/\partial z) = \zeta(\partial f/\partial\zeta)$ has been employed. Because g_1 and g_2 are assumed to be functions of ζ, f must be a function of ζ. Hence, $h = 1$ can be satisfied provided equation (12) holds and f is only a function of ζ (but f does not have to be identically zero). While the requirement of f being only a function of ζ agrees with expectation from MOST, it was not explicitly assumed. Instead, this outcome was derived from the heat flux budget equation when enforcing the constant flux assumption. Naturally, the constant flux assumption is common to both the derivation here and MOST. However, the f dependence on ζ is required by MOST but not the heat flux budget used here.

2.2. Linking *f* to Ejections and Sweeps

As earlier noted, f can be linked to asymmetry in ejections and sweeps contributions to F_s using quadrant analysis and the incomplete third-order cumulant expansion method (ICEM) (Cava et al., 2006; Katul, Kuhn, et al., 1997; Katul, Hsieh, et al., 1997; Nagano & Tagawa, 1988, 1990; Poggi et al., 2004). This expansion results in (Cava et al., 2006)

$$f = 2\sqrt{2\pi}\frac{\Delta S_o\phi_{ww}}{\gamma}, \tag{13}$$

where $\Delta S_o \in [-1, 1]$ is the fractional scalar flux imbalance between sweeps and ejections (sweeps minus ejections) and $\gamma = M_{21}/M_{12} - 1$ where $M_{21} = \overline{\theta'^2 w'}/(\sigma_\theta^2\sigma_w)$, $M_{12} = \overline{\theta' w'^2}/(\sigma_\theta\sigma_w^2)$, and σ refers to the standard deviation of a flow variable. To use equation (13) when $\overline{w'\theta'} > 0$, an axis transformation is needed as discussed elsewhere (Cava et al., 2006; Katul, Kuhn, et al., 1997; Katul, Hsieh, et al., 1997). It is clear that γ is a ratio formed by a dimensionless turbulent transport of F_s (i.e., $\overline{w'^2\theta'}/(\sigma_w^2\sigma_\theta)$) and a dimensionless turbulent transport of the scalar variance (i.e., $\overline{w'\theta'^2}/(\sigma_w\sigma_\theta^2)$). While equation (13) seems to suggest that f has a singularity when $\gamma = 0$, it is noted that ΔS_o also becomes zero when $\gamma = 0$ (i.e., sweep contributions to F_s are balanced by their ejection counterparts and the turbulent transport is completely symmetric) (Katul, Kuhn, et al., 1997).

The fact that the constant flux layer can exist without requiring $f = 0$ suggests that a constant flux layer may impose constraints on ΔS_o and γ that have not been previously realized. It has been shown that a constant flux layer with finite nonlocal transport described by equation (12) requires f to be only a function of ζ. Hence, ΔS_o and γ must also be functions of ζ. Are ΔS_o and γ only functions of ζ when the constant flux condition is a priori imposed?

More importantly, how far is $\kappa_v\zeta(\partial f/\partial\zeta)$ from zero? While imposing the constant flux condition does not require $\kappa_v\zeta\partial f/\partial\zeta = 0$, the significance of $\kappa_v\zeta(\partial f/\partial\zeta) = 0$ is twofold: first, it is a "sufficient" condition for the flux to be constant in the ASL (see Text S1 in the supporting information); second, in a constant flux layer it indicates that the vertical gradient of $\overline{w'w'\theta'}$, which appears directly in the flux budget equation (i.e., equation (3), is identically zero. The latter is because in a constant flux layer, one can express

$$\frac{\kappa_v z}{u_*\overline{w'\theta'}}\frac{\partial\overline{w'w'\theta'}}{\partial z} = \kappa_v\zeta\frac{\partial f}{\partial\zeta}. \tag{14}$$

A $\kappa_v\zeta(\partial f/\partial\zeta) = 0$ is automatically satisfied when $\zeta = 0$ (neutral ASL). As instability increases, the change in f with respect to ζ depends on how ϕ_{ww}, ΔS_o, and γ all covary with ζ. Among these three terms, ϕ_{ww} has been extensively studied (Garratt, 1992; Wyngaard, 2010) and is often expressed as $\phi_{ww} = a(1 - b\zeta)^{1/3}$, where a and b are similarity constants to be determined from field data. The "one-third" power law scaling for ϕ_{ww} stems

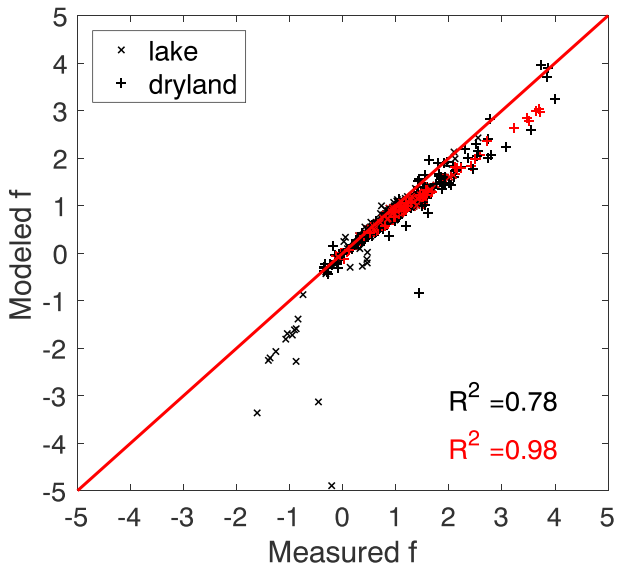

Figure 1. The comparison between measured and modeled f for θ. The data are from the lake site (crosses) and the dryland site (pluses). The black markers represent cases when no control is imposed on turbulent flux variations with z among the four levels, and the red markers represent cases when fluxes among the four levels have to be within 5% (10%) of each other at the lake (dryland) site.

from the fact that u_* should become dynamically unimportant under convective conditions (Kader & Yaglom, 1990). The variations of the other two variables (ΔS_o and γ) with ζ are less studied.

3. Data

The analysis makes use of two eddy covariance data sets. One data set was collected over a uniform lake surface (with minimal wave height), and the other was collected over a dryland shrub surface. These two data sets are chosen because each has eddy covariance measurements at four different levels in the ASL so that the constant flux layer assumption can be experimentally verified or data selection can be conditioned on it. The lake data set has measurements at 1.65, 2.30, 2.95, and 3.65 m (Bou-Zeid et al., 2008; Vercauteren et al., 2008). The dryland data set has measurements at 2, 8, 16, and 64 m (Finn, Clawson, et al., 2016; Finn, Reese, et al., 2016). The site characteristics, instrument details, and quality checks were presented in prior studies (Li & Bou-Zeid, 2011; Li et al., 2012, 2015; Finn et al., 2016, 2016) and are not discussed here. The computation of turbulent fluxes follows the methodology described in Li and Bou-Zeid (2011). For each 30 min data segment, linear detrending and double rotation are first applied to the measured time series. The Webb correction is applied to the computed latent heat flux (LE) and CO_2 flux. Data segments that satisfy the following conditions are discarded: (1) the mean wind originates from the back of the tower, (2) sensible heat flux (H), latent heat flux (LE), and u_* are too small (H<5W/m^2, LE<5W/m^2, u_*<0.05 m/s). In addition, only data collected under unstable conditions are included here given the interest in possible interactions between the ASL and the overlying CBL. At the lake site, the measured H is consistent across all four levels. For example, if the constant flux layer is defined as that turbulent fluxes at the four levels are within 5% of each other, there is a significant amount of data segments that satisfy this requirement. At the dryland site, flux variations among the four levels are larger partly because the magnitude of the sensible heat fluxes were 2–5 times larger than their lake counterpart. The H still satisfies the constant flux layer assumption if the previously assumed 5% criterion is increased to 10%. After the constant flux layer condition is imposed, no height dependence was found at the 95% confidence level for the sensible heat fluxes at both sites. Using regression analysis, the similarity coefficients $a=1$ and $b=4$ were determined by fitting ϕ_{ww} to measurements of the two data sets (see Figure S1 in the supporting information).

4. Results

First, ICEM predictions of f from equation (13) are compared with measured $f(=\overline{w'w'\theta'}/(u_*\overline{w'\theta'}))$. This is needed as a number of assumptions were made to arrive at equation (13) as discussed elsewhere (Cava et al., 2006; Katul, Kuhn, et al., 1997; Katul, Hsieh, et al., 1997). Figure 1 shows such comparison for two cases: (1) when no control is imposed on turbulent flux variations with z among the four levels (represented by black markers) and (2) when fluxes among the four levels have to be within 5% (10%) of each other at the lake (dryland) site (represented by red markers). The agreement between the ICEM approximation and measurements is acceptable ($R^2 = 0.78$ and $R^2 = 0.95$ for cases 1 and 2, respectively), lending support to the use of equation (13) for modeling f. This finding is consistent with previous studies showing that the ICEM captures ΔS_o under a variety of landscapes (Katul et al., 2006), including highly heterogeneous urban terrain (Wang et al., 2014). The comparison for q at the lake site is presented in Figure S3 in the supporting information, and the agreement is also acceptable.

The links between the constant flux layer, ΔS_o, and γ are explored next. We choose to impose sequentially more stringent criteria for defining a constant flux layer. Figure 2 shows ΔS_o (left) and γ (right) for $s = \theta$ using the lake data. The four different rows represent four situations: (1) no control is imposed on turbulent flux variations with z among the four levels (Figures 2a and 2b), (2) fluxes among the four levels have to be within 50% of each other (Figures 2c and 2d), (3) fluxes among the four levels have to be within 10% of each other (Figures 2e and 2f), and (4) fluxes among the four levels have to be within 5% of each other (Figures 2g and 2h). It is clear that as the criteria for "constant" flux become more stringent (from Figures 2a to 2g), the scatter

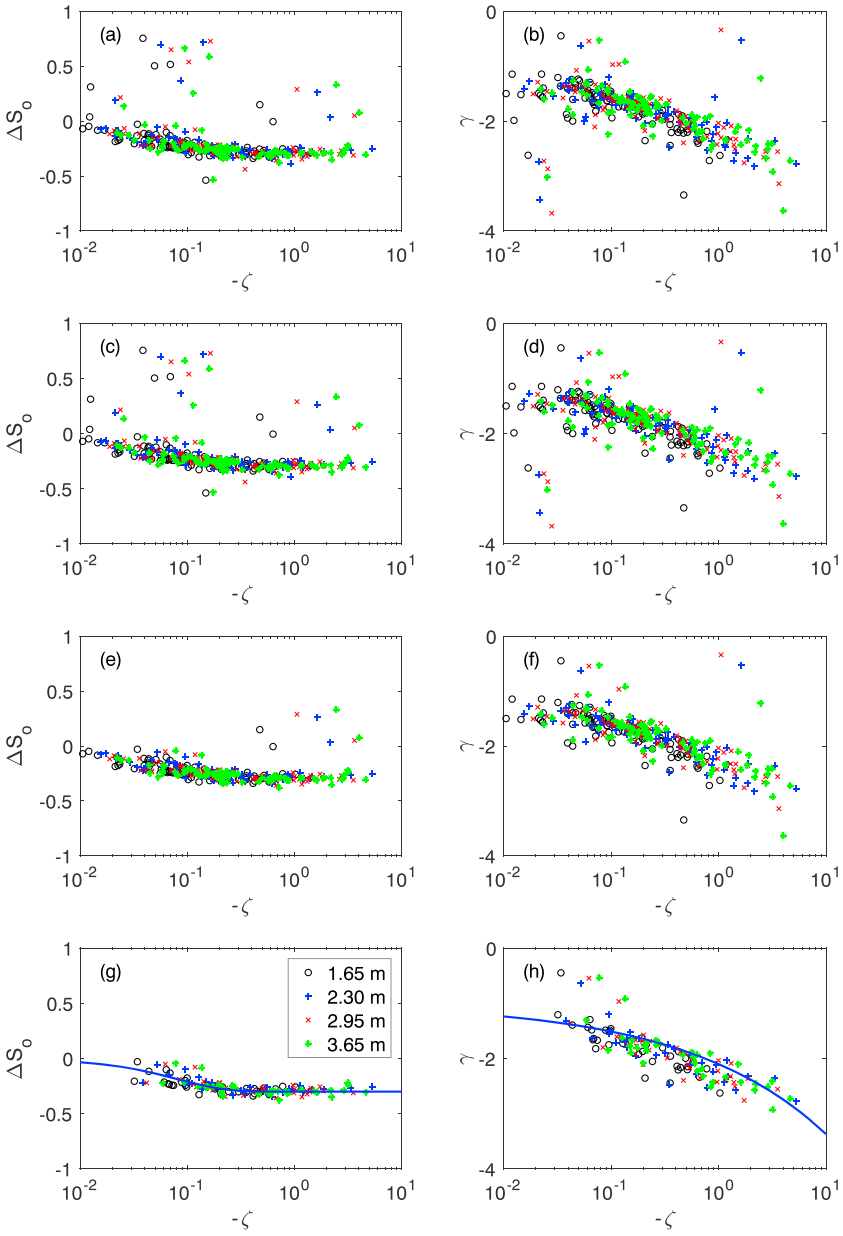

Figure 2. The ΔS_o (a, c, e, and g) and γ (b, d, f, and h) for θ at the lake site when (a and b) no control is imposed on turbulent flux variations among the four levels, (c and d) fluxes among the four levels have to be within 50% of each other, (e and f) fluxes among the four levels have to be within 10% of each other, and (g and h) fluxes among the four levels have to be within 5% of each other. The fitted blue lines in (g) and (h) are $\Delta S_o = 0.3\left[e^{12\zeta} - 1\right]$, $\gamma = -1.1\,(-\zeta)^{1/3} - 1$.

in ΔS_o and γ is reduced. Both variables become unambiguous functions of ζ when measured F_s among the four levels have to be within 5% of each other (Figures 2g and 2h). This finding is also supported by measurements for other scalars (e.g., q) at the lake site (see Figure S4 in supporting information) and measurements of θ at the dryland site (see Figure S5 in supporting information). Note that the ϕ_{ww} follows MOST expectations even when there is no control on flux variations among the four levels (see Figure S1).

We now show that imposing a constant flux layer does not require $\kappa_v\zeta(\partial f/\partial\zeta) = 0$ under all instability conditions. However, at the two extremes (i.e., neutral and convective conditions), $\kappa_v\zeta(\partial f/\partial\zeta) = 0$ is satisfied. Again, $\kappa_v\zeta(\partial f/\partial\zeta) = 0$ is automatically satisfied under neutral conditions since $\zeta = 0$. Under convective conditions ($\zeta \to -\infty$), ΔS_o approaches a constant (−0.3) and γ scales with $(-\zeta)^{1/3}$, as shown in Figures 2g and 2h, when measured H at the four levels are within 5% of each other (i.e., when the constant flux layer assumption is best

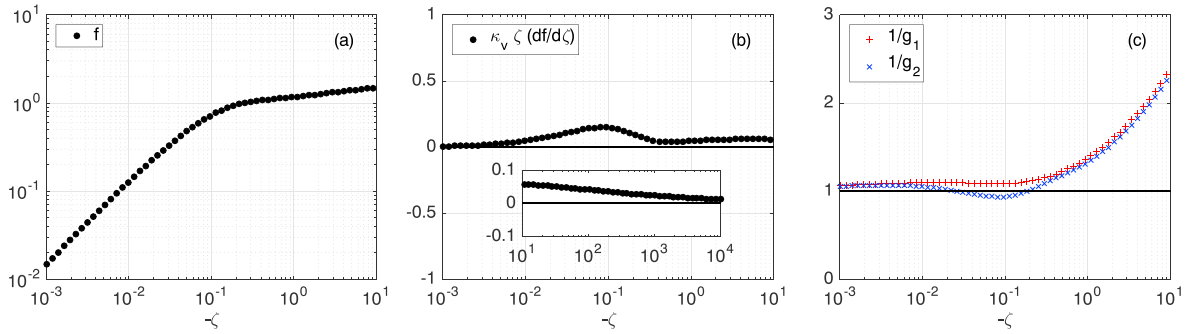

Figure 3. (a) f, (b) $\kappa_v\zeta(\partial f/\partial\zeta)$, and (c) $1/g_1$ and $1/g_2$ computed based on fitted functions in Figures 2g and 2h. The inset in (b) shows $\kappa_v\zeta(\partial f/\partial\zeta)$ in the range of $10<-\zeta<10^4$ to emphasize the fact that $\kappa_v\zeta(\partial f/\partial\zeta)$ approaches zero under convective conditions. To obtain g_1 and g_2, the following functions are also needed: $\phi_h=(1-16\zeta)^{-1/2}$, $\phi_{\theta\theta}=(-\zeta)^{-1/3}$, and $\alpha=2/3$ (Garratt, 1992; Ghannam et al., 2017). While other functional forms for ϕ_h and $\phi_{\theta\theta}$ and other values for α have been used, it is noted that ϕ_h, $\phi_{\theta\theta}$, and α only affect g_1 and g_2 but do not affect the results of f.

satisfied). As a result, $\Delta S_o\phi_{ww}/\gamma$ approaches a constant at large instabilities. Given that $f=2\sqrt{2\pi}(\Delta S_o\phi_{ww}/\gamma)$, it is expected that f also approaches a constant and thus $\partial f/\partial\zeta$ approaches zero under convective conditions, as shall be seen later.

Previous studies showed that ΔS_o approaches a constant under convective conditions in the ASL (Katul, Kuhn, et al., 1997; Li & Bou-Zeid, 2011). In addition, earlier work showed that M_{21} and M_{12} vary with instability. For example, using fitted MOST functions for normalized $\overline{\theta'^2w'}$ and $\overline{w'^2\theta'}$ in Kader and Yaglom (1990), Katul, Kuhn, et al. (1997) showed that M_{21} and M_{12} reduce to constants in the dynamic sublayer, dynamic-convective sublayer, and free convective sublayer of the ASL. While they obtained different constants in the three sublayers, they did not report a one-third power law scaling of M_{21}/M_{12} with respect to ζ. This difference is related to the experimental challenge of obtaining accurate third-order turbulent statistics (M_{21} and M_{12}) over a 30 min averaging interval while maintaining stationarity. As can be seen in Figure 2, the variability in γ remains significant even when the constant flux layer condition is best satisfied. Other reasons for the scatter include that $\overline{\theta'^2w'}$ is a variance transport term, whereas $\overline{w'^2\theta'}$ is a flux transport term. Hence, any noise or weak trends in θ'^2 that differ from their counterparts in w'^2 contribute to the scatter in γ.

Based on the fitted functions for ΔS_o and γ shown in Figures 2g and 2h, which also capture the q data over the lake site and the θ data over the dryland site (see Figures S4 and S5), Figures 3a and 3b present the variations of f and $\kappa_v\zeta(\partial f/\partial\zeta)$ across all instability conditions, respectively. Note again that f is only a function of ζ in the constant flux layer. It is evident that f initially increases from zero with increasing instability, and then the increase of f with ζ becomes slower as near-convective conditions are approached. The increase in f leads to a positive $\kappa_v\zeta(\partial f/\partial\zeta)$, which according to equation (14) indicates positive or upward turbulent flux transport under unstable conditions consistent with previous studies (Garratt, 1992; Stull, 1988). The fact that $\kappa_v\zeta(\partial f/\partial\zeta)$ is nonzero (except under neutral and convective conditions) implies that a near constant flux layer is compatible with a nonzero turbulent flux transport term. However, the value of $\kappa_v\zeta(\partial f/\partial\zeta)$ does approach 0 under near-convective conditions, as can be inferred from the observed saturation of ΔS_o and the $(-\zeta)^{1/3}$ scaling of γ with increasing instability. This finding suggests that to maintain a constant flux layer under near-convective conditions, the turbulent transport term in the flux budget equation must be zero. Together, these results demonstrate that a constant flux layer is harder to attain under convective conditions as it requires the turbulent flux transport term to be identically zero. Figure 3c further shows the calculated g_1 and g_2. Deviation of g_2 from g_1 caused by a finite turbulent flux transport term is nearly an order of magnitude smaller than g_1 itself, with the maximum deviation occurring around $-\zeta=0.1$ where ΔS_o starts to reach its saturation value. This result suggests that the relaxation time scale of the slow component of the pressure-scalar interaction term is not appreciably impacted by a finite turbulent flux transport term (at least in the constant flux layer).

5. Conclusions and Discussion

A constant scalar flux with z does not necessarily require $\overline{w'w'\theta'}=0$ as predicted from conventional gradient diffusion closure schemes for the aforementioned triple moment. The $\partial F_s/\partial z=0$ in the ASL leads to a novel

and possibly universal description of the imbalance between ejecting and sweeping eddy contributions to F_s (i.e., ΔS_o) with increasing instability. Specifically, for near-neutral conditions, $\Delta S_o \approx 0$ (symmetry), whereas ΔS_o saturates at ≈ -0.3 as near-convective conditions are approached (maximum asymmetry). Moreover, $\partial F_s/\partial z = 0$ leads to similarity in the ratio (i.e., γ) formed by a dimensionless turbulent transport of F_s (i.e., $\overline{w'^2\theta'}/\sigma_w^2\sigma_\theta$) and a dimensionless turbulent transport of the scalar variance (i.e., $\overline{w'\theta'^2}/\sigma_w\sigma_\theta^2$). This ratio appears to only vary with the atmospheric stability parameter ζ and scales with $(-\zeta)^{1/3}$ under convective conditions when enforcing $\partial F_s/\partial z = 0$ in the ASL.

A structural parameterization for the third-order transport term is shown to lead to $\overline{w'w'\theta'} = fu_*\overline{w'\theta'}$, where $f = 2\sqrt{2\pi}\Delta S_o\phi_{ww}/\gamma$. In the constant flux layer, this structural parameterization results in $\kappa_v z/(u_*\overline{w'\theta'})(-\partial\overline{w'w'\theta'}/\partial z) = \kappa_v\zeta\partial f/\partial\zeta$. Hence, the aforementioned universal patterns for ΔS_o and γ can be used to model the turbulent flux transport term in the constant flux layer or compare it to other terms in the budget equation. Interestingly, measured variations in ΔS_o and γ with respect to ζ lead to positive and nonzero values of $\kappa_v\zeta\partial f/\partial\zeta$, highlighting that a near constant flux layer does not necessarily require the turbulent flux transport term to be identically 0. However, the fact that $\kappa_v\zeta\partial f/\partial\zeta$ approaches 0 as the ASL becomes convective suggests that to maintain a constant flux layer under convective conditions, the turbulent flux transport term in the budget equation has to be zero.

Another implication of the work here is that single-level measurements of w' and θ' permit some diagnostic of the constant flux assumption. If the observed ΔS_o (determined from quadrant analysis) versus measured ζ falls on or near the curve provided here, then the constant flux assumption may be plausible. This finding is of practical significance given the lack of multilevel measurements of scalar fluxes in many field experiments and long-term monitoring initiatives. Future large eddy simulation studies are well suited to assess the generality or deficiency of this finding.

Acknowledgments
Katul and Liu acknowledge support from the National Science Foundation (NSF-EAR-1344703, NSF-AGS-1419614, NSF-AGS-1644382, and NSF-DGE-1068871) and from the Department of Energy (DE-SC0011461). We thank M. Parlange for sharing the lake data and D. Finn, S. Beard, T. Strong, B. Reese, E. Russell, and Z. Gao for assistance in the field campaign at the dryland site. The data can be obtained from the Environmental Fluid Mechanics group website of Boston University (http://sites.bu.edu/efm/data/).

References

Abdella, K., & McFarlane, N. (1997). A new second-order turbulence closure scheme for the planetary boundary layer. *Journal of the Atmospheric Sciences*, *54*(14), 1850–1867.

Baldocchi, D., Falge, E., Gu, L., Olson, R., Hollinger, D., Running, S., … Wofsy, S. (2001). Fluxnet: A new tool to study the temporal and spatial variability of ecosystem–scale carbon dioxide, water vapor, and energy flux densities. *Bulletin of the American Meteorological Society*, *82*(11), 2415–2434.

Bou-Zeid, E., Vercauteren, N., Parlange, M., & Meneveau, C. (2008). Scale dependence of subgrid-scale model coefficients: An a priori study. *Physics of Fluids*, *115106*(11).

Canuto, V., Minotti, F., Ronchi, C., Ypma, R., & Zeman, O. (1994). Second-order closure PBL model with new third-order moments: Comparison with LES data. *Journal of the Atmospheric Sciences*, *51*(12), 1605–1618.

Cava, D., Katul, G., Scrimieri, A., Poggi, D., Cescatti, A., & Giostra, U. (2006). Buoyancy and the sensible heat flux budget within dense canopies. *Boundary-Layer Meteorology*, *118*(1), 217–240.

Fer, I., McPhee, M. G., & Sirevaag, A. (2004). Conditional statistics of the Reynolds stress in the under-ice boundary layer. *Geophysical Research Letters*, *31*, L15311. https://doi.org/10.1029/2004GL020475

Finn, D., Clawson, K. L., Eckman, R. M., Liu, H., Russell, E. S., Gao, Z., & Brooks, S. (2016). Project Sagebrush: Revisiting the value of the horizontal plume spread parameter σ_y. *Journal of Applied Meteorology and Climatology*, *55*(6), 1305–1322. https://doi.org/10.1175/JAMC-D-15-0283.1

Finn, D., Reese, B., Butler, B., Wagenbrenner, N., Clawson, K., Rich, J., … Liu, H. (2016). Evidence for gap flows in the Birch Creek Valley, Idaho. *Journal of the Atmospheric Sciences*, *73*(12), 4873–4894.

Francone, C., Katul, G. G., Cassardo, C., & Richiardone, R. (2012). Turbulent transport efficiency and the ejection-sweep motion for momentum and heat on sloping terrain covered with vineyards. *Agricultural and Forest Meteorology*, *162*, 98–107.

Garratt, J. (1992). *The atmospheric boundary layer*. Cambridge: Cambridge University Press.

Ghannam, K., Duman, T., Salesky, S. T., Chamecki, M., & Katul, G. (2017). The non-local character of turbulence asymmetry in the convective atmospheric boundary layer. *Quarterly Journal of the Royal Meteorological Society*, *143*(702), 494–507.

Gryanik, V. M., & Hartmann, J. (2002). A turbulence closure for the convective boundary layer based on a two-scale mass-flux approach. *Journal of the Atmospheric Sciences*, *59*(18), 2729–2744.

Holtslag, A., & Boville, B. (1993). Local versus nonlocal boundary-layer diffusion in a global climate model. *Journal of Climate*, *6*(10), 1825–1842.

Holtslag, A., & Moeng, C.-H. (1991). Eddy diffusivity and countergradient transport in the convective atmospheric boundary layer. *Journal of the Atmospheric Sciences*, *48*(14), 1690–1698.

Kader, B. A., & Yaglom, A. M. (1990). Mean fields and fluctuation moments in unstably stratified turbulent boundary-layers. *Journal of Fluid Mechanics*, *212*, 637–662.

Katul, G., Hsieh, C.-I., Kuhn, G., Ellsworth, D., & Nie, D. (1997). Turbulent eddy motion at the forest-atmosphere interface. *Journal of Geophysical Research*, *102*, 13,409–13,421.

Katul, G., Kuhn, G., Schieldge, J., & Hsieh, C.-I. (1997). The ejection-sweep character of scalar fluxes in the unstable surface layer. *Boundary-Layer Meteorology*, *83*(1), 1–26.

Katul, G., Leuning, R., Kim, J., Denmead, O., Miyata, A., & Harazono, Y. (2001). Estimating CO_2 source/sink distributions within a rice canopy using higher-order closure model. *Boundary-Layer Meteorology*, *98*(1), 103–125.

Katul, G., Poggi, D., Cava, D., & Finnigan, J. (2006). The relative importance of ejections and sweeps to momentum transfer in the atmospheric boundary layer. *Boundary-Layer Meteorology*, *120*(3), 367–375.

Katul, G., Porporato, A., Manes, C., & Meneveau, C. (2013). Co-spectrum and mean velocity in turbulent boundary layers. *Physics of Fluids*, *25*, 091702.
Katul, G., Porporato, A., Shah, S., & Bou-Zeid, E. (2014). Two phenomenological constants explain similarity laws in stably stratified turbulence. *Physical Review E: Covering Statistical, Nonlinear, Biological, and Soft Matter Physics*, *89*(1), 023007.
Li, D., & Bou-Zeid, E. (2011). Coherent structures and the dissimilarity of turbulent transport of momentum and scalars in the unstable atmospheric surface layer. *Boundary-Layer Meteorology*, *140*(2), 243–262.
Li, D., Bou-Zeid, E., & de Bruin, H. (2012). Monin-Obukhov similarity functions for the structure parameters of temperature and humidity. *Boundary-Layer Meteorology*, *145*(1), 45–67.
Li, D., Katul, G., & Bou-Zeid, E. (2015). Turbulent energy spectra and cospectra of momentum and heat fluxes in the stable atmospheric surface layer. *Boundary-Layer Meteorology*, *157*(1), 1–21.
Mellor, G. L., & Yamada, T. (1974). A hierarchy of turbulence closure models for planetary boundary layers. *Journal of the Atmospheric Sciences*, *31*(7), 1791–1806.
Mellor, G. L., & Yamada, T. (1982). Development of a turbulence closure model for geophysical fluid problems. *Reviews of Geophysics*, *20*(4), 851–875.
Meyers, T. P., & Paw U, K. T. (1987). Modelling the plant canopy micrometeorology with higher-order closure principles. *Agricultural and Forest Meteorology*, *41*(1–2), 143–163.
Moeng, C.-H., & Wyngaard, J. C. (1986). An analysis of closures for pressure-scalar covariances in the convective boundary layer. *Journal of the Atmospheric Sciences*, *43*(21), 2499–2513.
Monin, A., & Obukhov, A. (1954). Basic laws of turbulent mixing in the ground layer of the atmosphere. *Trudy Akademiya Nauk SSSR Geofizicheskogo Instituta*, *151*, 163–187.
Nagano, Y., & Tagawa, M. (1990). A structural turbulence model for triple products of velocity and scalar. *Journal of Fluid Mechanics*, *215*, 639–657.
Nagano, Y., & Tagawa, M. (1988). Statistical characteristics of wall turbulence with a passive scalar. *Journal of Fluid Mechanics*, *196*, 157–185.
Poggi, D., & Katul, G. (2007). The ejection-sweep cycle over bare and forested gentle hills: A laboratory experiment. *Boundary-Layer Meteorology*, *122*(3), 493–515.
Poggi, D., Katul, G., & Albertson, J. (2004). Momentum transfer and turbulent kinetic energy budgets within a dense model canopy. *Boundary-Layer Meteorology*, *111*(3), 589–614.
Pope, S. (2000). *Turbulent flows*. Cambridge, UK: Cambridge University Press.
Rotta, J. (1951). Statistical theory of nonhomogeneous turbulence. *Zeitschrift für Physik*, *131*, 51.
Siqueira, M., & Katul, G. (2002). Estimating heat sources and fluxes in thermally stratified canopy flows using higher-order closure models. *Boundary-Layer Meteorology*, *103*(1), 125–142.
Stensrud, D. (2007). *Parameterization schemes: Keys to understanding numerical weather prediction models*. Cambridge: Cambridge University Press.
Stull, R. (1988). *An introduction to boundary layer meteorology*. Dordrecht: Kluwer Academic Publishers.
van Dop, H., & Verver, G. (2001). Countergradient transport revisited. *Journal of the Atmospheric Sciences*, *58*(15), 2240–2247.
Vercauteren, N., Bou-Zeid, E., Parlange, M. B., Lemmin, U., Huwald, H., Selker, J., & Meneveau, C. (2008). Subgrid-scale dynamics for water vapor, heat, and momentum over a lake. *Boundary-Layer Meteorology*, *128*(2), 205–228.
Wallace, J. M. (2016). Quadrant analysis in turbulence research: History and evolution. *Annual Review of Fluid Mechanics*, *48*, 131–158.
Wang, L., Li, D., Gao, Z., Sun, T., Guo, X., & Bou-Zeid, E. (2014). Turbulent transport of momentum and scalars above an urban canopy. *Boundary-Layer Meteorology*, *150*(3), 485–511.
Wyngaard, J. C. (1985). Structure of the planetary boundary layer and implications for its modeling. *Journal of Applied Meteorology and Climatology*, *24*(11), 1131–1142.
Wyngaard, J. C. (2010). *Turbulence in the atmosphere*. New York: Cambridge University Press.
Wyngaard, J. C., & Weil, J. C. (1991). Transport asymmetry in skewed turbulence. *Physics of Fluids*, *3*(1), 155–162.
Yamada, T. (1975). The critical Richardson number and the ratio of the eddy transport coefficients obtained from a turbulence closure model. *Journal of the Atmospheric Sciences*, *32*, 926–933.
Zilitinkevich, S., Gryanik, V. M., Lykossov, V., & Mironov, D. (1999). Third-order transport and nonlocal turbulence closures for convective boundary layers. *Journal of the Atmospheric Sciences*, *56*(19), 3463–3477.